

# CASE STUDIES IN ROOT CAUSE ANALYSIS: IDENTIFYING OPPORTUNITIES FOR IMPROVED MAINTENANCE OF CANDU FUELLING MACHINES

M. SCHIPPKE, K. ELLISON, A. JÄRVINE<sup>1</sup>, and K. PICKLES<sup>2</sup>

## ABSTRACT

The charge tube assembly of the CANDU® fuelling machine contains numerous moving/rotating components (ball screws, linear and rotating bearings, mechanical gears, mechanical seals, etc). Premature wear-out and/or failure of key charge tube components can result in the need for unscheduled or excessively frequent overhauls and repairs, along with its associated negative effects. This paper presents two examples of root cause investigations involving the charge tube and ram assembly.

The first case study details the metallurgical failure examination of a failed ram assembly that fractured at the threaded connection between a ram drive screw and ram extension tube. The failure was discovered several hours after the ram was driven manually to a stall condition in response to ram encoder errors. Detailed metallurgical examinations of the failed ram identified the primary fracture mode as stress corrosion cracking, which occurred during the application of a sustained tensile and torsional load while the ram was in the full retract position. Difficulties encountered during installation of the dowel pin resulted in the formation of microcracks, which subsequently grew by stress corrosion cracking. This was the root cause of the failure.

In the second case study, the fuelling machine (FM) head H5B at Bruce B was taken out of service for a partial overhaul. At that time, it was discovered that the charge tube rear ball nut had sustained excessive ball wear damage which appeared to be confined to only one groove. The damaged charge tube ball nuts, balls, deflectors, and ball return tubes were examined. The rear charge tube ball nuts displayed evidence of alternating or intermittent wear on the outboard surfaces of the front and rear ball tracks. In contrast, the front ball nut exhibited more uniform and less severe wear of the ball tracks. A wear mechanism is presented that is consistent with the observed damage pattern. The proposed wear mechanism is based on the assumption that the balls are not free to move along the ball track as the ball screw is rotated. The wear experienced by the ball nuts results in a loss of pre tension, affecting the fine positioning of the charge tube.

In each case, the root cause analysis determined that there were opportunities for improvements in maintenance practices that will improve the overall reliability and performance of the fuelling machines at Bruce Power.

KEYWORDS: Root cause analysis, fuelling machine, ram balls, ram drive screw, stress corrosion cracking

## INTRODUCTION

The charge tube assembly of the CANDU® fuelling machine contains numerous moving/rotating components (ball screws, linear and rotating bearings, mechanical gears, mechanical seals, etc). Premature wear-out and/or failure of key charge tube components can result in the need for unscheduled or excessively frequent overhauls and repairs, with its associated negative effects: maintenance costs,

---

<sup>1</sup> Materials and Component Health Department, Generation Life Cycle Management, Kinectrics, Inc, 800 Kipling Avenue, Toronto, Ontario, M8Z 6C4 ([michelle.schippke@kinectrics.com](mailto:michelle.schippke@kinectrics.com), [keith.ellison@kinectrics.com](mailto:keith.ellison@kinectrics.com), [allan.jarvine@kinectrics.com](mailto:allan.jarvine@kinectrics.com))

<sup>2</sup> Section Manager, Fuel Handling Technical, Bruce Power, Tiverton, Ontario, N0G 2T0 ([Kevin.pickles@brucepower.com](mailto:Kevin.pickles@brucepower.com))

® CANDU is a registered trademark of Atomic Energy of Canada Limited

® CANDU is a registered trademark of Atomic Energy of Canada Limited

radiation exposure, reduced fuelling rates, and upsets to the general head overhaul schedule. Major functional failures while the machine is locked on channel (e.g., unable to install the closure plug) poses a major economic risk that could result in millions of dollars of lost revenue. Thus, whenever a fuelling machine component or sub-system does not perform as expected, there is an urgent need to identify the problem and implement appropriate corrective actions to improve the overall system safety, reliability, and plant performance. This paper presents two examples of root cause investigations involving the charge tube and ram assembly.

## **1. CASE STUDY #1: H6B BALL SCREW FAILURE**

### **1.1 Introduction**

On February 23, 2008, the H6B fuelling machine (FM) was fuelling Unit 5 channel H17 at Bruce B and finished accepting two bundles when the charge tube was retracted into the FM head to store the fuel carrier. At this time, the ram encoder started to produce shaft encoder errors even though the ram was not being driven. The ram was then manually retracted to a stall using minimum speed and torque to allow the charge tube to release from the fuel carrier. The ram brakes were engaged and the ram was left in the stall condition while Bruce Power Control Maintenance and Fuel Handling Technical personnel assessed the ram encoder errors. The ram was left in the stall condition for over 3 hours (but the actual time may have been greater than 6 hours) and subsequent disassembly of the machine revealed that the ram assembly had failed at the fine-threaded connection where the ram drive screw connects to the ram extension tube. Kinectrics was called on-site to aid in the troubleshooting efforts and asked to perform the subsequent metallurgical failure investigation of the H6B ram ball screw. The failed ram ball screw was received at Kinectrics Radiation Laboratory (KRL) and a rapid response investigation was initiated.

The ball screw is manufactured by Thomson Saginaw Ball Screw Co., and the ball screw material is procured through Carpenter Technology Corporation. Manufacturing test certificates provided by Carpenter indicated that the ball screw was manufactured according to AMS 5617 Rev H Grade 1 and ASTM A564-04 Grade XM-16 in the H950 condition. The manufacturer's test certificates showed that the ball screw conformed to the chemistry, cleanliness, and mechanical properties specified. The ball screw was installed new into the H6B charge tube/ram assembly during the first quarter of 2006 and placed into service in March 2006.

## **1.2 RESULTS AND DISCUSSION**

### **1.2.1 Macroscopic Examination**

Photographs of the failed H6B Ram Ball Screw are shown in Figure 1.1. The images show the fracture of the ball screw within the extension tube and on the ball screw side. During assembly, the ball screw is threaded into the ram extension tube followed by drilling and reaming of the dowel hole and insertion of the dowel pin.

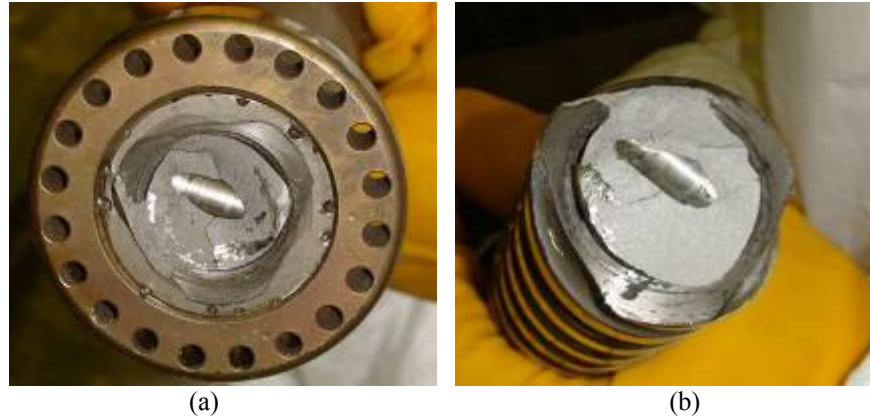


Figure 1.1: Field photographs taken of the failed ram ball screw. Figure 1a shows the ram extension tube side of the fracture and Figure 1b shows the ball screw side of the fracture.

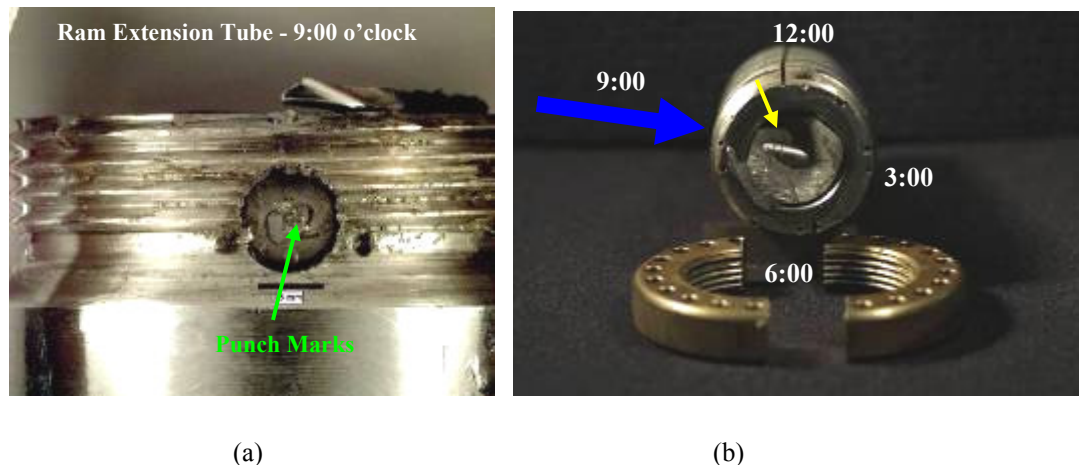


Figure 1.2: Laboratory photographs taken of the fracture surface within the ram extension tube following removal of the ring (a). Figure 1.2(b) illustrates the clock positions given to the dowel pin entrances for reference and the groove marks observed on the pin (yellow arrow).

Figure 1.2a illustrates the punch marks observed on the dowel pin, indicating the direction from which the pin was driven into the ram extension tube and ball screw assembly (9:00 o'clock). Circumferential grooves were observed on the dowel pin toward the 9:00 o'clock position (see yellow arrow in Figure 1.2a). The clock positions are slightly skewed so that the 3:00 o'clock and 9:00 o'clock correspond to the dowel hole openings. The large blue arrow shows the suspected direction of force applied to the ram tube during the staking of the dowel pin.

Thread damage was observed on the ram extension tube and the ball screw at the dowel hole entrances. In particular, the edges of the threads, at the entrance of both ends of the dowel hole in the ball screw, sustained obvious mechanical damage, characterized by plastic deformation. Cracks were observed, emanating from both ends of the dowel hole, which were linked to the primary fracture surface (Figure 1.3). A small secondary crack was also identified emanating from a thread root at the dowel hole entrance at the 3:00 o'clock position (Figure 1.3b&c).

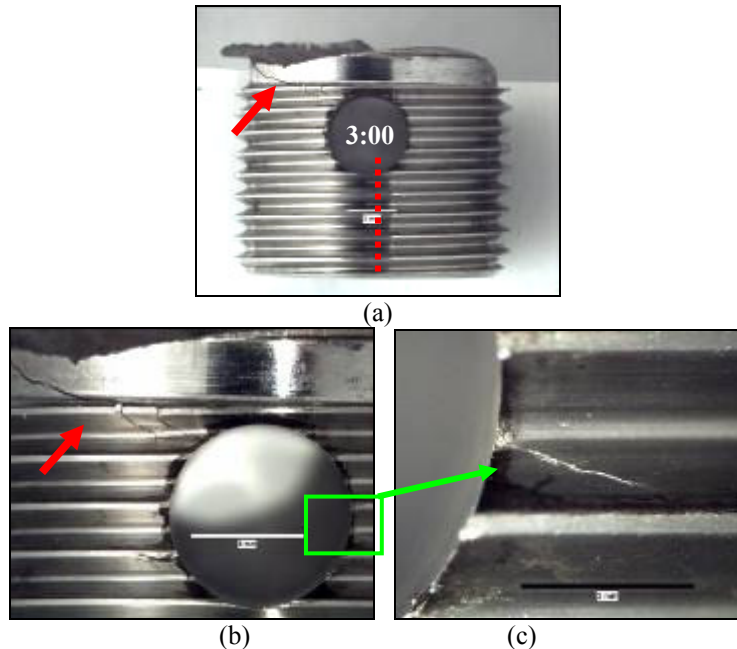


Figure 1.3: Macro images of the dowel hole entrance on the ball screw at the 3:00 o'clock position. The red arrows highlight the primary fracture. The boxed region in (b) is shown at higher magnification in (c).

#### 1.2.2 Scanning Electron Microscopy (SEM) Examination of the Ball Screw Threads

High magnification, secondary electron images of the damage observed on the threads at the 3:00 o'clock position, looking from the inside surface of the dowel hole, are shown in Figures 1.4 and 1.5. Cracks were found emanating from the thread roots and fracture surfaces were present on the thread flanks. Microscopic examination of the fracture surface morphology revealed the presence of transgranular cleavage facets (Figure 1.4b). Within the fracture surfaces, debris was observed buried within the deformed and fractured region at the root of one of the threads (Figure 1.4c). The debris appeared as curly, metal shavings, and the shape and morphology of the shavings are consistent with metal turnings produced by reaming operations. Elemental analysis of the debris revealed that the debris had a very similar composition as the ball screw base material.

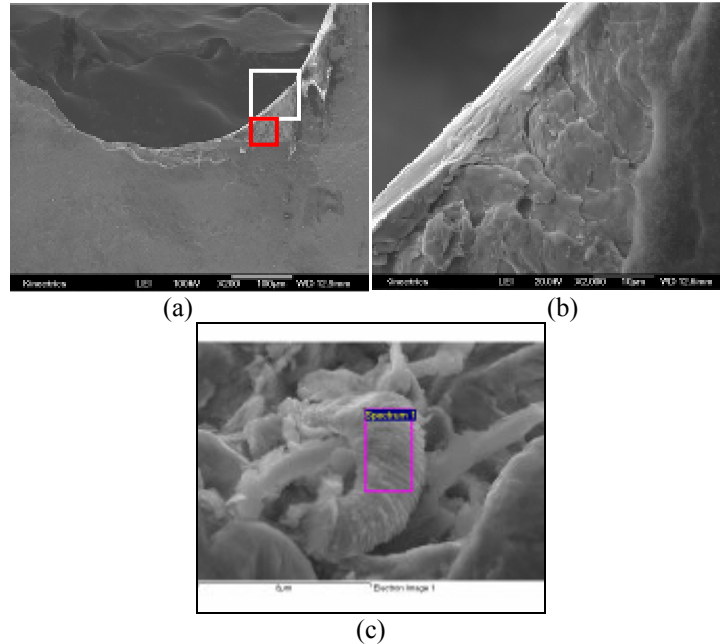


Figure 1.4: Secondary electron images of a crack observed at a thread root on the inside diameter of the dowel hole at the 3:00 o'clock position. The white boxed region is shown at higher magnification in (b). The red boxed region is shown at higher magnification in Figure 11c.

Representative SEM images of the thread damage observed on the threads at the 9:00 o'clock position are shown in Figure 1.5. Smear and folded over metal observed on the thread faces and at the thread root suggest that the threads at the dowel hole sustained mechanical damage.

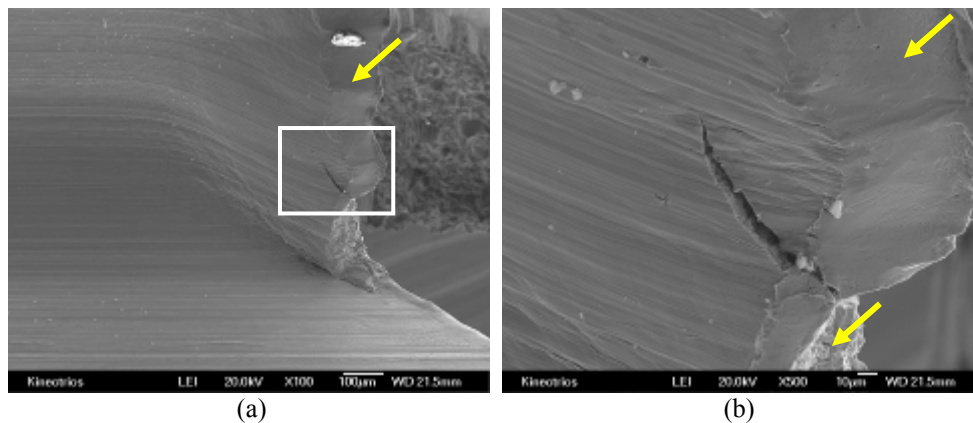


Figure 1.5: Secondary electron images of one of the threads at the 9 o'clock position, showing thread deformation (yellow arrows) and secondary cracking emanating from the thread face. The image shown in (b) is a higher magnification image of the boxed region in (a).

### 1.2.3 Dowel Pin Examination

Circumferential wear marks were observed at the ends of the pin where the pin contacts the ID of the dowel hole inside the ball screw at the 3:00 and 9:00 o'clock position. A cylindrical projection of the pin surface, highlighting the rolled-in grooves and mechanical damage observed around the circumference of the pin, is shown in Figure 1.6. Areas of wear and mechanical damage were observed towards the 3:00 o'clock and 9:00 o'clock ends of the dowel pin surface.

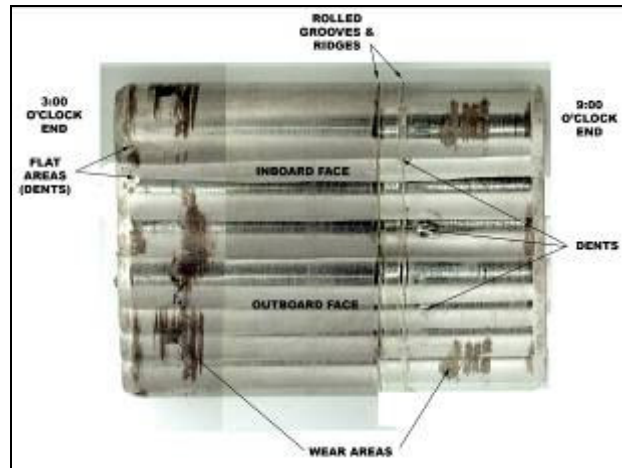


Figure 1.6: Cylindrical projection of the dowel pin surface, highlighting the rolled-in grooves and mechanical damage observed on the pin surface.

Diameter measurements of the dowel pin and ram extension tube dowel hole ID, taken with a calliper at the 3:00 o'clock and 9:00 o'clock positions, were performed and compared against the design diameter of the pin ( $0.3132'' \pm 0.0003^3$ ). The measurements showed that the dowel hole diameter exceeded the design diameter of  $0.3125'' \pm 0.0002$  at all positions measured. The measured diameter of the dowel hole in the ball screw averaged  $0.3169'' \pm 0.0004$  at the 3:00 o'clock position and  $0.3173'' \pm 0.0004$  at the 9:00 o'clock position, both being significantly greater than the design dowel hole diameter.

The dowel pin fit was compared with the ram extension tube and the ball screw respectively. The data showed that the pin had a clearance fit of  $0.0024''$  at the inserted end and an even greater clearance fit of  $0.0031''$  at the driven end of the extension tube. The pin has a clearance fit of  $0.0028''$  with the dowel hole in the ram ball screw. These measurements are consistent with an over-sized dowel hole that was simultaneously reamed through both the extension tube and the ball screw. Furthermore, the measurements show that the pin should have fit loosely into the dowel hole. However, it was noted that, during reinsertion of the pin at the 3:00 o'clock position of the ram extension tube, additional force was required to overcome resistance offered by material protruding from the ID surface of the hole. Punch marks, observed on the inside of the dowel hole within the extension tube, were the cause of the protrusion.

Macro examination of the tapered ends of the pin revealed the presence of mechanical damage, which may have caused the diameter of the pin at this location to be reduced. Diameter measurements taken at indents on the tapered end of the 3:00 o'clock position (identified as flat areas or dents in Figure 1.6) revealed that the pin diameter was mechanically reduced by  $0.0054''$ .

#### 1.2.4 Ball Screw Fracture Surface Examination

The extension tube side of the fracture surface was cut axially up to the dowel hole, as shown by the dotted line in Figure 1.3a, to facilitate further examination of the dowel hole ID and primary crack origins. Once the piece was cut, the fracture surface was opened into two pieces, which for reference purposes, were labeled A-side and B-side (Figure 1.7).

<sup>3</sup> Calculated dimension, corresponding to an interference fit of  $0.0002 - 0.0012''$ .

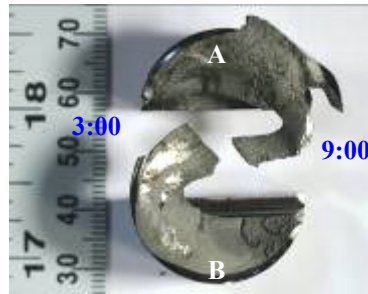


Figure 1.7: Photograph of the fracture surface of the ball screw pertaining to the extension-tube side of the fracture.

Macro image of the B-side fracture surface at the crack origin site at the 9:00 o'clock position is shown in Figure 1.8. A thumbnail crack, characterized by the dark radial stain (arrow of Figure 1.8), was observed at the intersection of the dowel hole and threads. High magnification examination of the fracture surface morphology, using SEM, was performed at the regions highlighted by the boxes in Figure 1.8. Energy Dispersive Spectroscopy (EDS) examinations of the crack origin region revealed the presence of carbon-based deposits on the fracture surface. The carbon deposits obscured the features of the underlying fracture.

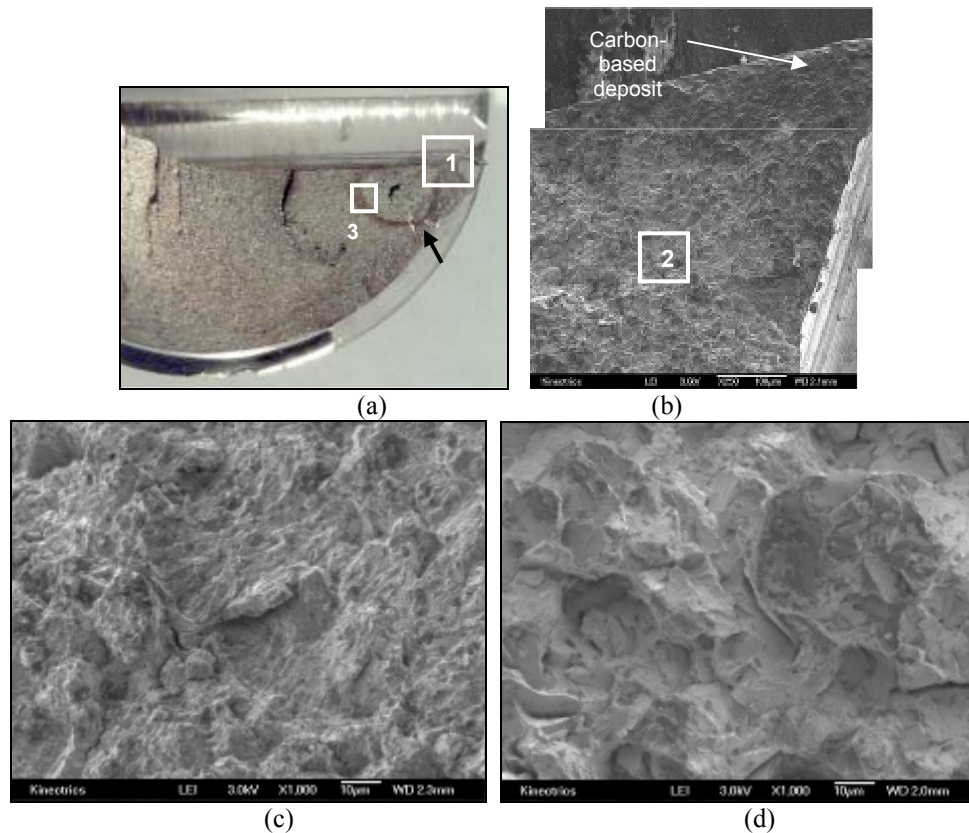


Figure 1.8: Macro image of the B-side fracture surface at the crack origin site, 9:00 o'clock position, detailing the locations where high magnification SEM analysis of the fracture surface was performed (a). Secondary electron images of the crack origin; the image shown in (b) corresponds to box 1, the image shown in (c) corresponds to box 2, and the image shown in (d) corresponds to box 3.

Just beyond the carbon deposit, the fracture surface exhibited intergranular features followed by a narrow zone of transgranular cleavage. Beyond the narrow zone of transgranular cleavage, the fracture

morphology was characteristic of intergranular crack propagation. Beyond the latter and through to final separation of the ball screw, crack growth was predominantly by transgranular fracture.

### 1.2.5 Metallographic Examination and Characterization of the Ball Screw

A photograph of the ball screw fracture surface, following sectioning, is shown for reference in Figure 1.9a. The arrow in the image points to the cross-sectional plane used for metallography shown in Figures 1.9b-e. The axial section shows a large crack, which propagated parallel to and beneath the main fracture surface (Figure 19.b). The crack contains several branches and its tortuous propagation path suggests that the crack propagated in an intergranular mode (Figure 1.9c). After etching, the intergranular crack propagation path was confirmed, Figure 1.9 d&e.

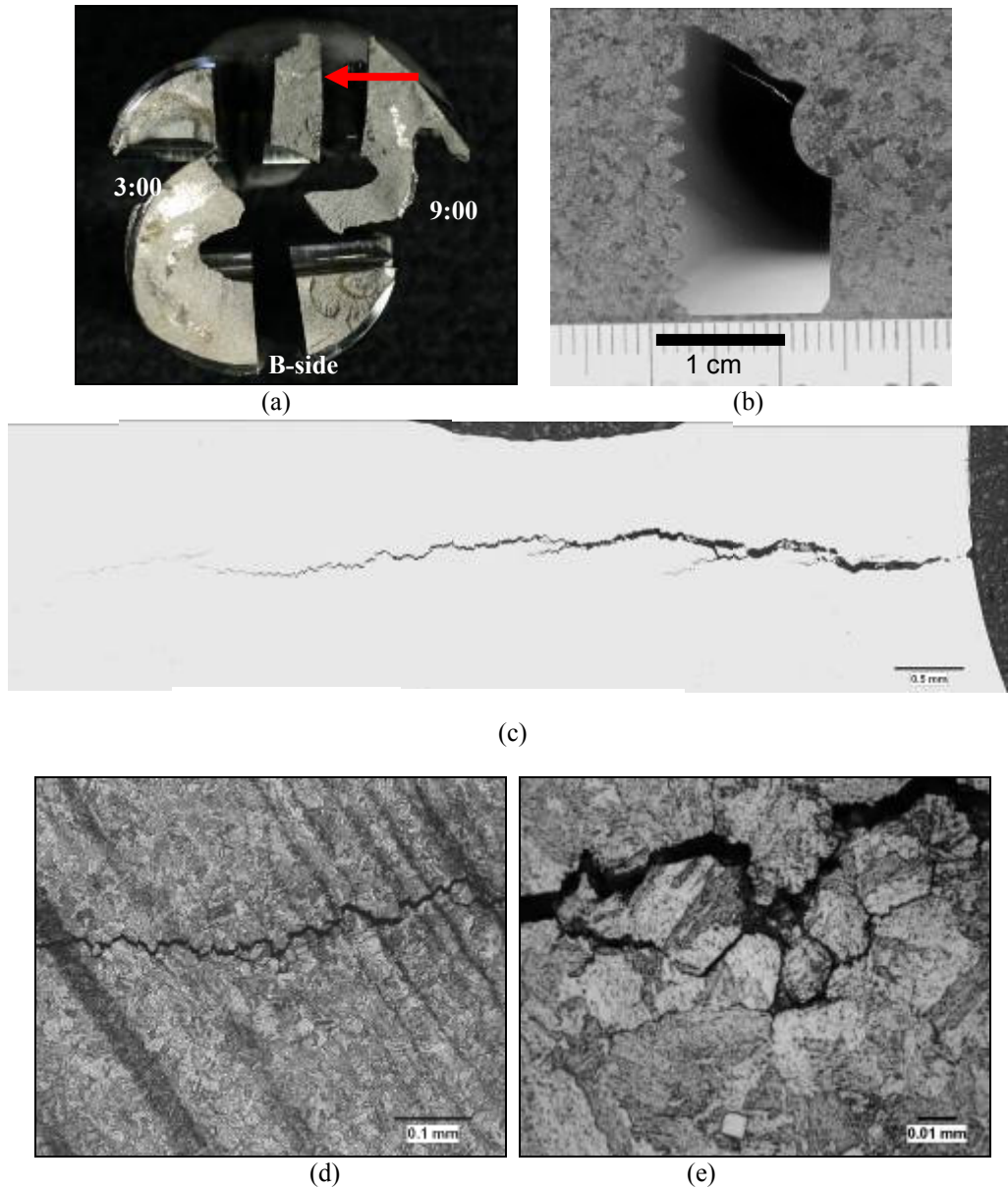


Figure 1.9: The cutting plan of the ball screw fracture surface for metallographic examination is shown in image (a). Image (b) shows the cross-sectional plane examined in (c) through (e). Optical micrographs of the crack, before and after etching, are shown in image (c) and (d&e) respectively.

Characterization of the ball screw base material was performed. Chemical analysis by inductively-coupled plasma (ICP) was performed on the ram ball screw bulk material and indicated that the material was in conformance with Custom 455, as detailed in the specification [1]. Optical micrographs of the base metal microstructure in the transverse direction are shown in Figure 1.10. The base metal microstructure consists of a banded, martensitic structure. With the exception of the banding, the microstructure is typical of Custom 455® alloy.

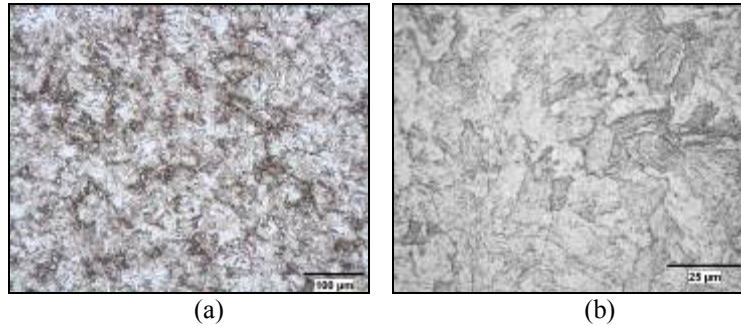


Figure 1.10: Optical micrographs of the bulk microstructure in the transverse direction. Image (b) is a higher magnification image of a representative region of (a).

Vickers microhardness measurements were performed in the bulk cross-section and on the ram ball screw side of the fracture surface. The microhardness measurements taken of the bulk material ranged from 471 HVN (min) to 497 HVN (max), with an overall average of 483 HVN, which is equivalent to 48 Rockwell C (HRC). These measurements were performed on a transverse section of the ball screw material.

Microhardness measurements taken on the ball screw side of the fracture surface were higher than those taken of the bulk material. The highest measurements were noted closer to the 9:00 o'clock position of the dowel hole and ranged from 505 HVN (min) to 548 HVN (max), with an overall average of 528 HVN, which corresponds to 51 HRC.

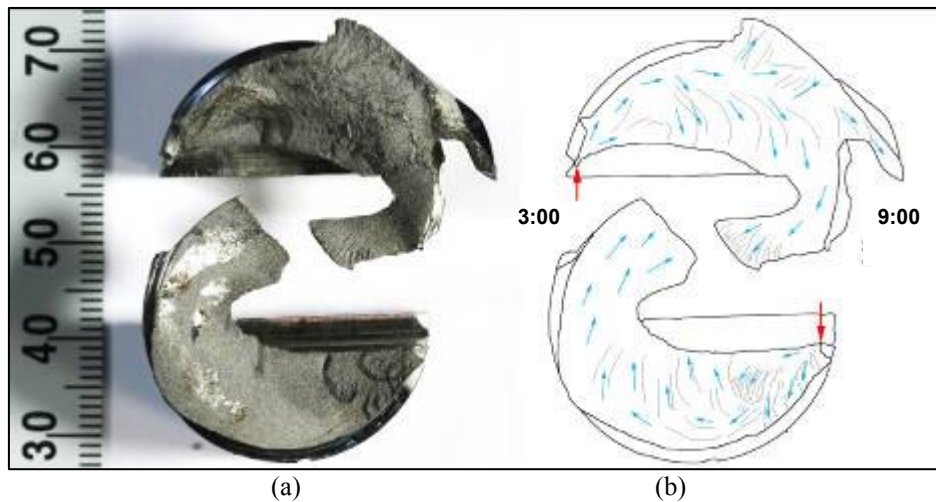


Figure 1.11: Macro image of fracture surface (a) and applied loading diagram (b). The red arrows point to the primary fracture origins where the dowel pin contacted the dowel hole and damage was imparted to the threads during installation. The blue arrows highlight the direction of crack growth, which led to the final failure of the ball screw.

## 1.3 CONCLUSIONS AND RECOMMENDATIONS

### 1.3.1 Failure Mechanism

Given the circumstances of the failure, and the evidence collected from this investigation, the metallurgical cause of the failure was identified as intergranular stress corrosion cracking (IGSCC), initiated from previously formed microcracks located at the intersection of the dowel hole with the ball screw threads.

Stress corrosion cracking (SCC) is the brittle failure, at relatively low constant tensile stress, of an alloy exposed to a corrosive environment [2]. Intergranular SCC is characterized by preferential attack and fracture of the grain boundaries in the alloy in question. Three conditions must be present simultaneously to produce SCC: a critical environment, a susceptible alloy, and some component of tensile stress.

Thumbnail cracks, characterized by radial stains emanating from the crack origins, indicate that a corrosion process was occurring at the crack propagation front. It is suspected that the stains and dark deposits observed at the crack origins is one of the lubricants, Anchorlube® or Never-Seez® NG165, used during the installation of the ram extension tube assembly. Data developed in recent years indicates more and more that stress corrosion cracking in high strength steels is caused by hydrogen [3]. It is likely that the hydrocarbons present in the lubricant were the source of the hydrogen driving embrittlement at the crack tip. High magnification SEM examination of the fracture surface morphology revealed that, in the early and stable stages of growth, the crack propagated in an intergranular mode. In addition, metallographic examination of one of the primary cracks provided further evidence of an intergranular propagation mechanism. Numerous branches emanating from the primary crack further support IGSCC as the basis for crack propagation. In the H950 condition, Custom 455® material has the lowest (compared with other aging conditions) resistance to IGSCC.

At the crack origin on the B-side, 9:00 o'clock position, the sequence of crack propagation modes (i.e., intergranular/transgranular/intergranular) suggests that there was a shift from static to dynamic loading conditions during operation of the ball screw. The sustained loading condition caused by the manual stall of the ram provided the conditions for uninterrupted crack propagation by IGSCC until the crack grew to a critical size. At this point, the crack grew by transgranular cleavage.

### 1.3.2 Cause of Failure

The apparent root cause was attributed to improper procedures associated with the installation of a dowel pin during the overhaul of the charge tube in March 2006 and IGSCC. More specifically, micro-cracks were introduced around the entrance of the dowel hole in the ball screw during the insertion of a dowel pin. The IGSCC initiated from these micro-cracks. Literature states that tensile stresses, even below yield, are sufficient to cause SCC and may result from bolting and fastening parts that fit together imperfectly [2]. The ball screw suffered complete fracture as a result of the following contributing factors: (1) operator response to ram encoder errors on February 22, 2008 led to sustained static loads on the ram assembly, which promoted IGSCC (primary factor), (2) the ball screw alloy was aged to a condition that provided adequate hardness in this application, but did not provide optimal resistance to IGSCC (secondary factor), and (3) higher than expected hardness values point to insufficient time at temperature during aging of the ball screw alloy, resulting in an enhanced susceptibility to SCC (least significant factor).

### 1.3.3 Recommendations

Based on the unusual circumstances of the installation of the ram ball screw into the extension tube assembly, as well as the extended duration in which the ram was retracted and left in a manual stall condition following the ram encoder errors, failure of the H6B ram ball screw is believed to be an isolated event. However, due to the potential for the existence of similar defects in other charge tube assemblies, caused by similar installation procedures, the possibility of similar failures in other fuelling machine heads cannot be completely ruled out. To mitigate the risk of such failures, the following recommendations are made:

- Non-destructive examination of all existing and in-service ram assemblies should be performed to check for evidence of thread damage. Given the size of the pre-existing microcracks observed in this

investigation, crack-like flaws capable of initiating IGSCC may go undetected using conventional NDE methods. Consequently, the standard NDE examinations should be supplemented by replica examinations of the ball screw dowel holes at the next available overhaul. This action addresses the risk to other assemblies arising from the apparent root cause of the failure.

- Installation procedures regarding drilling and reaming the dowel hole into the ram extension tube and ball screw assembly, as well as the insertion of the dowel pin, require more specific trouble-shooting criteria when over-sized pins are encountered. Therefore, revision of the mechanical maintenance procedure is recommended as a means of mitigating future occurrences.
- Minimizing the amount of time the ram is spent in the full retract position during manual operations addresses the primary contributing factor to this failure.
- Carpenter Custom 455® precipitation-hardened stainless steel, in the H950 condition, is inherently susceptible to IGSCC. It is suggested that an alternate material, such as Custom 465®, be considered for this application. This addresses the second and the third contributing factors to the failure.

## 2.0 CASE STUDY #2: EXAMINATION OF DAMAGED BALL NUTS FROM FUELLING MACHINE HEAD H5B

### 2.1 Introduction

On May 13, 2006, fuelling machine (FM) head H5B at Bruce B was taken out of service for a partial overhaul. At that time it was discovered that the charge tube rear ball nut had sustained excessive ball wear damage that appeared to be confined to only one groove. Bruce Power staff noted that this was the same FM head that experienced the failure of the ram spline balls approximately three months earlier in February, 2006. The damaged charge tube ball nuts, balls, deflectors, and ball return tubes removed from H5B were sent to Kinectrics for metallurgical examination to assist in a root cause analysis of the damage to the ball nuts. Three ball nuts were sent to Kinectrics for examination: the front (S/N 84) and rear (S/N 92) ball nuts, removed from H5B in May 2006, and an older rear ball nut (S/N 96) with extensive ball wear damage for comparative purposes.

A drawing of the charge tube ball nuts is provided in Figure 2.1. The charge tube ball lead screw and nuts are manufactured from UNS-S45500 stainless steel to ASTM A-750-80 Type XM-16. The cobalt-base balls are investment castings manufactured from Haynes Stellite Star-J alloy. The ball deflectors are manufactured from type 440C high carbon martensitic stainless steel. When assembled, the front and rear ball nuts are separated by a Belleville washer which provides pre-tension on the ball nuts to aid in fine positioning of the charge tube during operation.

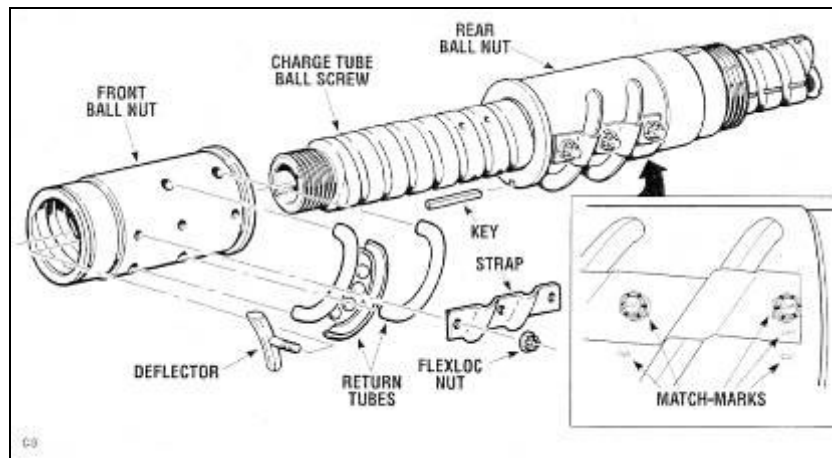


Figure 2.1: Drawing of the charge tube ball nuts and related hardware. The inboard (reactor) end is on the left.

## 2.2 RESULTS

### 2.2.1 Ball Nuts

Photographs of the interior of the damaged rear nut S/N 92 from H5B are shown in Figures 2.2. When viewed from the inboard end of the nut, there was obvious wear of the outboard surface of the rear ball track, as highlighted by arrows in Figure 2a. The damage comprised an intermittent or alternating pattern of heavy wear versus light wear along the length of the ball track, as highlighted by the arrows in Figure 2.2a. The damage was confined to the last  $\sim 300^\circ$  of the ball track, ending at the outboard exit hole. The angular width of the heavily worn areas was approximately  $12^\circ$ . In addition, the heavily worn areas were separated from each other by approximately  $12^\circ$ . Thus it appeared that the wear scars were introduced at alternating ball locations. It was noted that the  $12^\circ$  angular distance was roughly equal to the width of one individual ball. The damage did not appear to be caused by plastic deformation (or “Brinnelling”) of the ball tracks, since there was no evidence of deformation of the adjacent surfaces. When viewed from the outboard end of the nut, the inboard sides of the front and rear ball tracks did not show any evidence of wear. However, the outboard edges of all tracks were raised and sharpened, presumably due to wear caused by contact with the balls (Figure 2b).

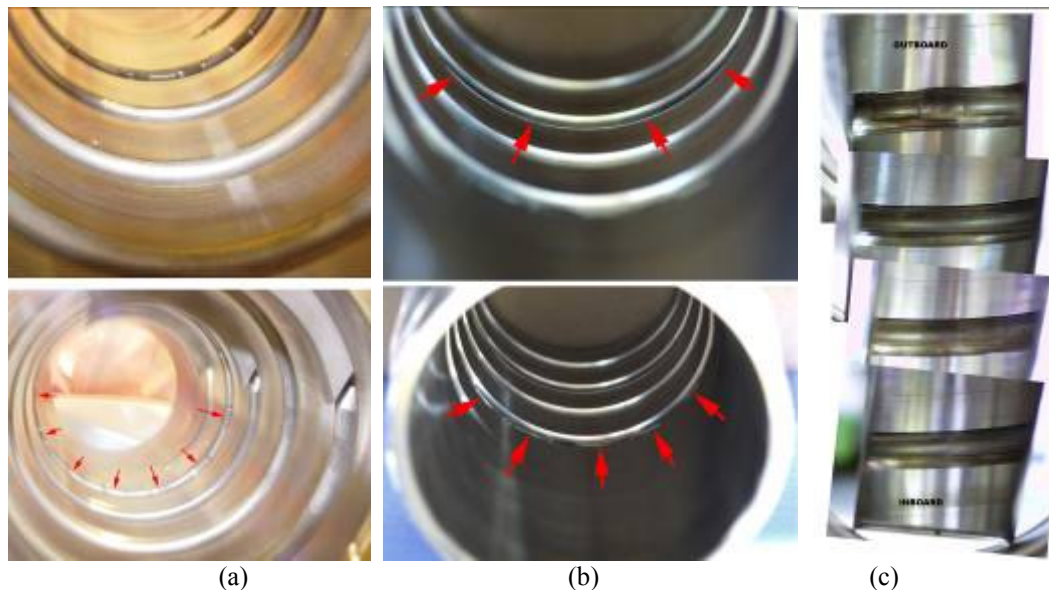


Figure 2.2: (a) Interior view of the rear ball nut S/N 92 from H5B, looking towards the outboard end (b) interior view of the rear ball nut S/N 92 from H5B, looking towards inboard end. (c) Mosaic image of the ball tracks on the left side of the nut, view looking outboard with the ball deflector stud holes facing up.

In contrast to the damage observed on the rear nut, the front nut (S/N 84) displayed only minor evidence of wear due to ball contact. The inboard edges of both ball tracks exhibited some sharpening and raised edges, presumably due to wear caused by contact with the balls.

Photographs of the older rear ball nut S/N 96 are shown in Figure 2.3. Localized wear areas on the outboard surfaces of the front and rear ball tracks are indicated by the red arrows. The inboard surfaces of the front and rear ball tracks did not show any evidence of wear. The outboard edges of the tracks were raised and sharpened due to deformation or wear caused by contact with the balls. Both the front and rear ball tracks of this rear nut displayed extensive wear on the outboard surfaces, with an alternating pattern similar to that observed on the H5B rear nut S/N 92. Once again, the damage comprised an intermittent or alternating pattern of heavy wear versus light wear along the entire length of each ball track.

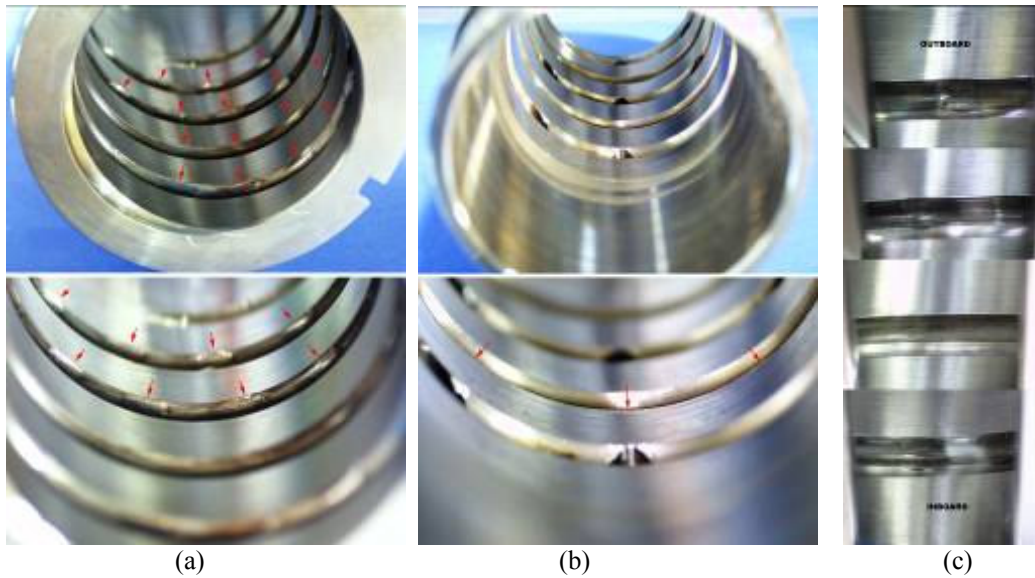


Figure 2.3: (a) Interior view of the older rear ball nut S/N 96, looking towards the outboard end. (b) Interior view of the older rear ball nut S/N 96, looking towards the inboard end. (c) Interior view of the older rear ball nut S/N 96. Mosaic image of the ball tracks on the bottom of the nut, with the ball deflector stud holes facing up.

The hardness of the three ball nuts was checked at three circumferential locations mutually offset by 120° and three axial locations, representing the two ends and the middle of the nut. Three additional readings were taken on one end face of each nut. Canadian General Electric Design Specification DS-29-35213 states that “no individual hardness reading shall be below 44 Rockwell C” and all hardness readings from the three ball nuts met the specification requirement. Moreover, there were no significant differences in the hardness between the three nuts.

2.2.2 Balls

Four sets of balls from the H5B front and rear nuts were provided for examination. All of the balls were dull and discoloured with tracking marks, but there were no obvious flat spots that would be an indication of ball skidding. Figure 2.4 presents the results of the measurements of ball diameter for all of the balls in all four sets.

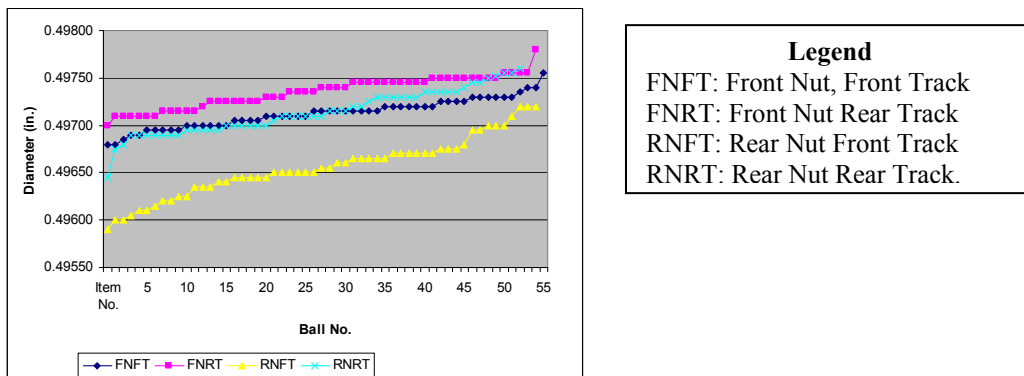


Figure 2.4. Diameter of the balls from the front and rear ball nuts from H5B.

The diameter of most of the front nut (front and rear tracks) and the rear nut rear track balls varied from approximately 0.4970 inches (12.624 mm) to 0.4975 inches (12.637 mm), representing a loss of between

0.0025 inches (0.064 mm) and 0.0030 inches (0.076 mm). In contrast, the diameter of the majority of the rear nut front track balls varied from approximately 0.4960 inches (12.598 mm) to 0.4970 inches (12.624 mm), representing a loss of between 0.0030 inches (0.076 mm) and 0.0040 inches (0.102 mm) in the diameter of the balls.

The hardness of the balls was checked by sampling five balls at random from each set. The GE Canada specification states that the hardness of the balls after stress relief shall be 56-63 Rockwell C. All hardness values were within the designer's specification range.

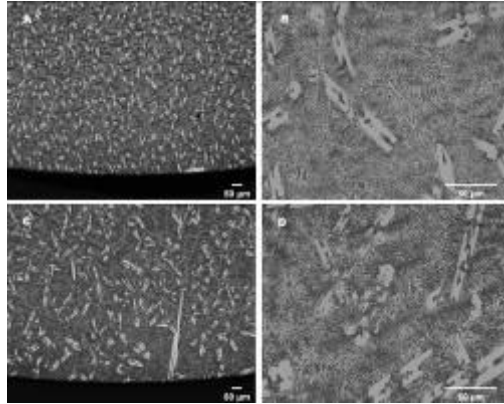


Figure 2.5: Optical micrographs obtained from two balls from H5B front nut S/N 84. A, B: front track; C, D: rear track.

Figure 2.5 shows representative optical micrographs from balls selected at random from each of the four sets. The balls displayed a cast microstructure, comprising carbides of varying length embedded in a cobalt-base matrix. In some of the cross-sections, the carbides were more elongated than in other sections (e.g., Figure 2.5c). None of the balls exhibited excessive micro-porosity.

### 2.2.3 Deflectors (H5B Nuts Only)

Each ball nut (front and rear) is fitted with three ball deflectors, located at the inboard, mid and rear positions. The deflectors from the front and rear H5B nuts were visually inspected, hardness assessed, and the length measured to check for conformance to Strite DWG D-102-484-1.

With the exception of the rear nut inboard deflector S/N 38, all of the deflectors showed evidence of wear on both ends of the deflectors. The right side of S/N 38 was unused. The maximum depth of ball wear (0.006 inches) was noted on the end of deflector S/N 38 (rear, inboard).



Figure 2.6: Photographs of rear nut S/N 92, inboard ball deflector S/N 38.

The total length of the deflectors was checked and compared to the requirements of Strite DWG D-102-484-1. All deflectors were found undersized by 0.003 to 0.010 inches. Note that the length measurements were made away from the areas exhibiting localized ball wear.

The hardness of the ball deflectors was measured and compared with the requirements of Canadian General Electric Design Specification DS-29-35213. The deflectors are initially furnace heat-treated to achieve a base hardness of 26-33 Rockwell C. The ends of the ball deflectors are subsequently hardened via an induction heating procedure to achieve design hardness in the range of 57-62 Rockwell C on the end faces. The hardness of the end faces was measured at the locations specified in Canadian General Electric Design Specification DS-29-35213. The hardness on the deflector end faces was generally in the low to mid 50's on the Rockwell C scale, somewhat below the design hardness range.

#### 2.2.4 Return Tubes

The ball return tubes were examined visually for evidence of wear and the remaining wall thickness was measured at various locations. There was evidence of wall thinning, especially at the bends.

#### 2.2.5 Ball Track Wear Depth Measurements

Measurements of ball track wear depth were obtained by preparing rubber impression molds of the front and rear ball nut ID surfaces. Note that since front ball nut S/N 84 did not exhibit visible localized wear, measurements of general front and rear ball track wear were made at the 180° orientation. The areas on rear ball nuts S/N 92 and S/N 96 that exhibited the most pronounced ball track wear are numbered and circled in Figure 2.7. These areas of the molds were sectioned transverse to the ball tracks so that the profiles of the worn and non-worn areas could be compared and measured. Figure 2.8 shows a representative pair of images, corresponding to worn and non-worn areas of the front ball track of rear ball nut S/N 96, and indicating the method of wear depth measurement.

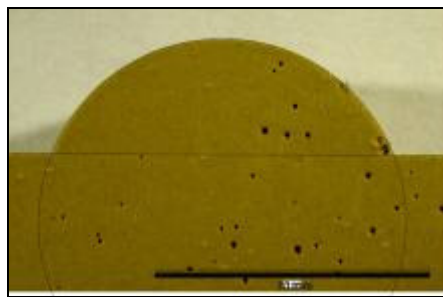


(a)

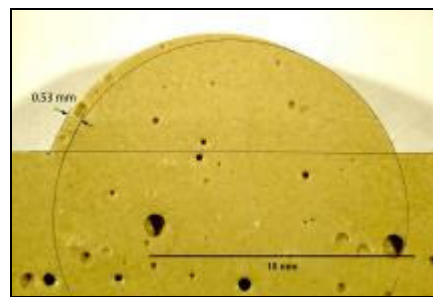


(b)

Figure 2.7: Photographs of the rubber impression mold used for measurement of ball groove wear depth in rear ball nut S/N 92 (a) and rear ball nut S/N 96 (b). Numbered circles indicate areas of enhanced wear.



Front Ball Track: 0°-30° Inboard



#7: Rear Ball Track: 150°-180° Inboard

Figure 2.8. Macro photographs of two sections cut from the rubber impression mold of rear ball nut S/N 96. The left image (a) is a non-wear region of the front ball track between the deflector stud hole and a ball return hole that was used as the reference standard for the original ball track profile. The right image (b) shows a region of the ball track exhibiting localized wear.

The maximum depth of localized wear was 1.02 mm (0.040 inches) in the rear ball track of rear ball nut S/N 92, approximately 180° opposite from the deflector stud holes. Rear ball nut S/N 96 exhibited localized wear as deep as 0.63 mm (0.025 inches) in both the front and rear ball tracks. Front ball nut S/N

84 exhibited more uniform wear of between 0.30 to 0.43 mm (0.012 to 0.017 inches) in the front and rear ball tracks.

## 2.2 DISCUSSION

### 2.2.1 Ball Nut Damage Mechanism

A sketch, illustrating a wear mechanism, which could explain the observed damage pattern on the two rear ball nuts, is presented in Figure 2.9.

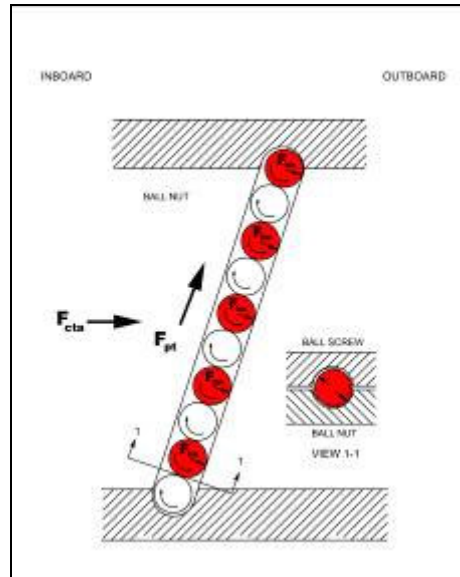


Figure 2.9: Sketch showing a cross section of a ball nut and a proposed arrangement of balls and forces that could produce the wear pattern observed on the two rear ball nuts.

The sketch represents a partial interior view of a rear ball nut and shows an arrangement of balls inside a 180° segment of one of the ball tracks. The wear model is based on the presumption that for some reason (yet to be determined), the balls are not free to move in one or both directions along the ball track(s) inside the ball nut. As the charge tube is advanced or retracted, the rotation of the ball screw relative to the ball nuts results in a compressive force,  $F_{pt}$ , on the chain of balls acting parallel to the ball track.

As shown in Figure 2.9, this compressive force results in the balls becoming jammed inside the ball tracks with an alternating pattern. The alternating arrangement of ball positions results in a certain component of  $F_{pt}$  being transmitted as a normal force between the balls and the surfaces of the ball track. Every second ball transmits a normal force,  $F_{bn}$ , onto the ball nut side of the track (red balls in Figure 2.9), whilst the remaining balls transmit an equal and opposite normal component of  $F_{pt}$  onto the ball screw side of the track. (Note that the ball screw is not shown in Figure 2.9). When the FM head is positioned at the outlet end of a fuel channel (i.e., fuelling against the flow, or de-fuelling with flow), the primary heat transport flow force produces an additional outward axial force on the charge tube (ball screw),  $F_{cta}$ . The axial flow force tends to roll the balls up the outboard side of the ball nut ball tracks and increases the magnitude of  $F_{bn}$ .

Finally, the rotation of the ball screw relative to the ball nuts causes the balls to rotate against the sides of the ball track. It is this rotation of the balls, as they are forced against the outboard surface of the ball track(s), but prevented from moving along it, that could explain the observed alternating surface wear pattern. The cobalt-based balls are harder than the Custom 455® alloy ball nuts, and would therefore tend to cause more wear on the ball nut surfaces.

## 2.3 CONCLUSIONS

A wear mechanism is presented that is consistent with the observed damage pattern on the ball nuts. The proposed wear mechanism is based on the assumption that the balls are not free to move along the ball track as the ball screw is rotated. As a result of the wear, the ball nuts loose pre-tension, affecting the fine positioning of the charge tube.

## SUMMARY

The charge tube assembly of the CANDU® fuelling machine contains numerous moving/rotating components (ball screws, linear and rotating bearings, mechanical gears, mechanical seals, etc). Premature wear-out and/or failure of key charge tube components can result in the need for unscheduled or excessively frequent overhauls and repairs, along with its associated negative effects. This paper presented two examples of root cause investigations involving the charge tube and ram assembly where opportunities for improved maintenance practices were identified. These improvements significantly impact the overall reliability and performance of fuelling machines at Bruce Power.

## ACKNOWLEDGEMENTS

The authors would like to acknowledge A. Cervoni, T. Ryans, S. Nixon, V. Duarte, and R. Gutthardt for carrying out the laboratory examinations.

## REFERENCES

- [1] A-705M, "Specification For Age-Hardening Stainless and Heat Resisting Steel Forgings", ASTM Specification, 1989.
- [2] Jones, D. "Principles and Prevention of Corrosion, Second Edition", Prentice Hall, 1996.
- [3] Henthorne, M. "Stress Corrosion Cracking of Martensitic Precipitation Hardening Stainless Steels", Carpenter Technology Corporation Reading, Pennsylvania 19603 USA.

---

® CANDU is a registered trademark of Atomic Energy of Canada Limited